# Stochastic analysis of a non-local fractional viscoelastic beam forced by Gaussian white noise

Gioacchino Alotta[a] and Mario Di Paola[a] and Giuseppe Failla[b] and Francesco P. Pinnola[c]
[a]Department of Civil, Environmental, Aerospace, Materials Engineering (DICAM), University of Palermo, Viale delle Scienze Ed. 8, 90128 Palermo, Italy.
[b]Departiment of Civil, Energy, Environment, Materials Engineering (DICEAM), University of Reggio Calabria, Via Graziella, Localit Feo di Vito, 89124 Reggio Calabria, Italy.
[c]Engineering and Architecture Faculty, University of Enna "Kore", Viale delle Olimpiadi, 94100 Enna, Italy.

**Abstract:** Recently, a displacement-based non-local beam model has been developed and the relative finite element (FE) formulation with closed-form expressions of the elastic and fractional viscoelastic matrices has also been obtained. The static and quasi-static response has been already investigated. This work investigates the stochastic response of the non-local fractional viscoelastic beam, forced by a Gaussian white noise. In this context, by taking into account the mass of the beam, the system of coupled fractional differential equations ruling the beam motion can be decoupled with the method of the fractional order state variable expansion and statistics of the motion of the beam can be readily found.

## 1 Introduction

In the last decades, the non-local beam theories have known a great interest. This is due to their ability to capture the mechanical behavior of beam-like micro- and nanodevices [1, 2] that avoid computationally expensive (and sometimes prohibitive) molecular simulations [3]; indeed the behaviour of such micro- and nano-elements can not be reproduced correctly by the classical local continuum approach [4].There are several non-local theories available in literature; the most known is for sure the Eringen's integral theory [5], successfully applied to Euler-Bernoulli (EB) model [6]; however there are many other effective theories used to construct non-local beams model. Although most of the works have been carried out to model the non-locality related to the pure stiffness, recently a great effort has been dedicated by researchers of the the field to the modeling of non-local damping effects. Indeed, recent studies demonstrate that non-local damping effects at microscale are relevant in application like image acquisition via high-speed atomic force microscopes [7] or frequency measurements of vibrating nanosensors [8]; damping effects have also been observed as a result of humidity and thermal effects [9] or external magnetic forces [10]. Applications of non local damping effects at macroscale also exists, see for examples [11, 12]. In the last years the authors have proposed non-local EB and TM beam models which treats non-local effects as long-range interactions depending on the relative motion of nonadjacent volume elements [13–16]. The model is suitable for finite element (FE) implementation and closed form of the FE formulation can be readily found [16]. Both elastic and fractional viscoelastic [17–19] long-range interactions have been included in this model [20]. In this paper the model has been further improved by taking into account the mass of the beam. Indeed this is the only way to evaluate the error in measurement of micro-/nanosensors or the error committed by micro-/nanoactuators due to environmental noise. In

first approximation the noise is modelled as Gaussian white noise. The coupled FE equations of motion with fractional derivative can be decoupled efficiently with the fractional order state variable expansion [21]. It is shown that all the elements of the power spectral density (PSD) matrix can be obtained in analytical form.

## 2 Non-local fractional viscoelastic model

In this section the mechanical model of non-local fractional viscoelastic beam is briefly introduced. Firstly, the basic concepts of fractional viscoelasticity are discussed, then the mechanical model of the non-local beam is introduced; finally, the finite element formulation is derived.

### 2.1 Fractional viscoelasticity

In this work, the viscoelastic forces are modelled by means of the tools of fractional calculus, that is a branch of mathematics that study the integro-differential operators of real order and their applications. In particular, fractional operators appear when power law creep/relaxation functions are assumed to describe the linear viscoelastic behaviour. Indeed, if we assume the relaxation function as follows

$$R(t) = \frac{C_\alpha t^{-\alpha}}{\Gamma(1-\alpha)} \tag{1}$$

where $0 \leq \alpha \leq 1$ and $C_\alpha$ are material parameters, while $\Gamma(\cdot)$ is the Euler gamma function, by substituting it in the integral form of the Boltzamann superpositon principle we obtain:

$$F(t) = \int_0^t R(t-\tau)\dot{u}(\tau)d\tau = \frac{C_\alpha}{\Gamma(1-\alpha)} \int_0^t (t-\tau)^{-\alpha}\dot{u}(\tau)d\tau = C_\alpha \left({}_0D_t^\alpha u\right)(t) \tag{2}$$

where $F$ is the force, $u$ is the displacement and $({}_0D_t^\alpha \cdot)$ is the Caputo fractional derivative. Eq. (2) is related to the case in which a displacement is applied and the resulting force is evaluated. If the force is applied, the creep function is used in the Boltzmann superpoistion principle and the inverse relationship of Eq. (2) is obtained in the following form

$$u(t) = \frac{1}{C_\alpha} \left({}_0I_t^\alpha F\right)(t) \tag{3}$$

where $({}_0I_t^\alpha \cdot)$ is the Riemann-Liouville fractional integral. Formore information abut fractional calculus and fractional viscoelasticity see [19].

### 2.2 Kinematic and local resultant of the beam

As shown in Fig. 1 the bar has an arbitrary cross section with area $A$, it is referred to an axis $x$ coincident with centroidal axis; the material of the beam is assumed linearly elastic characterized by the Young modulus $E$.
Under the assumptions of small displacements, the kinematics of the beam can be completely described by the following:

$$\chi(z) = -\frac{d\varphi(z)}{dz}; \quad \gamma(z) = \frac{dv(z)}{dz} - \varphi(z) \tag{4}$$

where $\chi$ is the curvature, $\varphi$ is the rotation of the transverse section about the $x$ axis, $v$ is the transverse displacement in $y$ direction and $\gamma$ is the shear strain. The local resultants are written as

$$T_y^{(l)}(z) = \int_A \tau_{xy}(x,y,z)dA = G^* K_s A\gamma(z); \quad M_x^{(l)}(z) = \int_A \sigma_z(x,y,z)ydA = E^* I_x \chi(z) \tag{5}$$

where $T_y^{(l)}$ is the local shear resultant in $y$ direction, $A$ is the area of the cross section, $\tau_{xy}$ is the shear stress, $K_s$ is the shear factor, $M_x^{(l)}$ is th local bending resultant, $\sigma_z$ is the local stress in the $z$ direction, $I_x$ is the moment of inertia about the $x$ axis, $E^* = \beta_1 E$, $G^* = \beta_1 G$ and $\beta_1$ is a dimensionless parameter with values in the range $0 \div 1$, that reduces the amount of local effects.

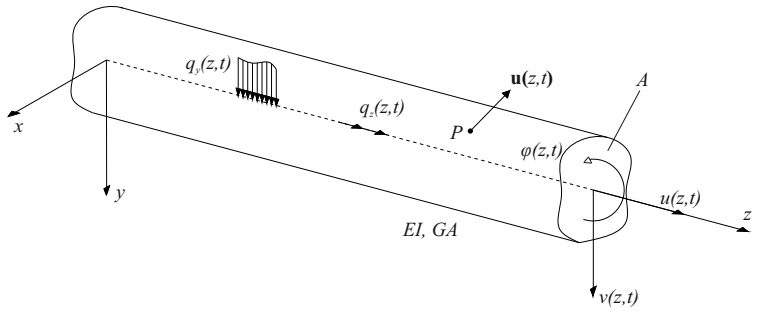


*Figure 1: Non local beam.*

## 2.3 Long-range forces

The non-local model is constructed under the assumption that non-adjacent bar segment mutually exert long-range viscoelastic forces due to relative motion. More specifically, consider two nonadjacent bar segment of volume $\Delta V(x_i)$ and $\Delta V(\xi_k)$ located at the positions $z = z_i$ and $z = \zeta_k$ on the bar axis, respectively; they mutually exert long-range forces and moments as a consequence of their relative motion measured as pure deformation [22]. The force are supposed to be self-equilibrated according to the Newton's third law. The long-range forces are written as linearly depending on the product of the two volumes and the attenuation function governing the decay of non-local effects with the relative distance; both purely elastic and fractional viscoelastic forces, modeled by Caputo's fractional derivative, are considered. A mechanical description of the long range interactions is depicted in Fig. 2.
The pure deformations $\theta$ and $\psi$ are defined as follows:

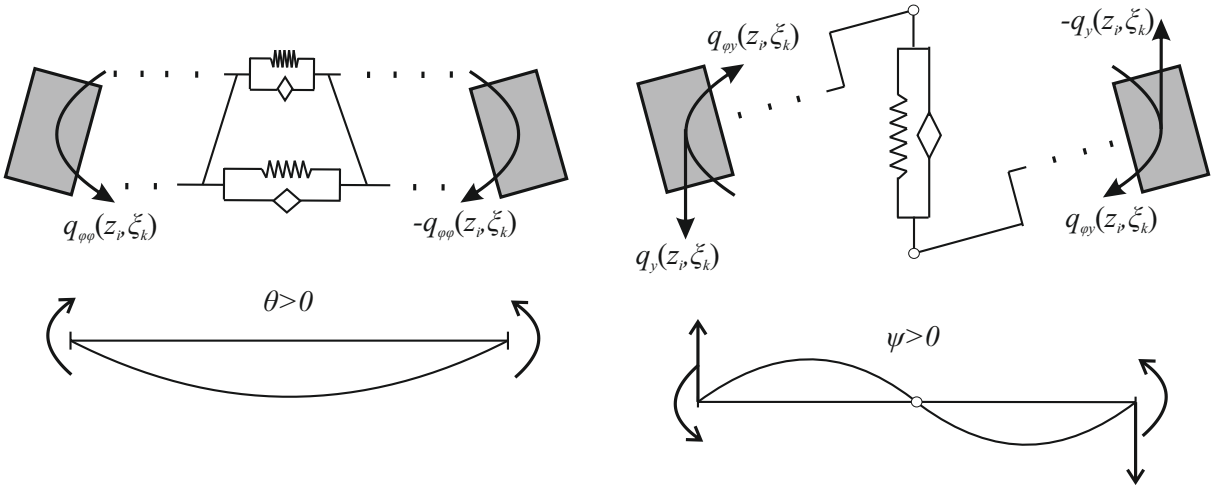


*Figure 2: Pure mode of deformation.*

$$\theta(z_i,\zeta_k) = \varphi(\zeta_k) - \varphi(z_i); \qquad \psi(z_i,\zeta_k,t) = \frac{v(\zeta_k,t) - v(z_i,t)}{\zeta_k - z_i} + \varphi(\zeta_k) + \varphi(z_i) \tag{6}$$

The bending moments mutually exerted by the two volumes $\Delta V(x_i)$ and $\Delta V(\xi_k)$, due to the pure bending rotation $\theta$, is given as:

$$q_{\varphi\varphi}(z_i,\zeta_k,t) = r_{\varphi\varphi}(z_i,\zeta_k,t) + d_{\varphi\varphi}(z_i,\zeta_k,t) \tag{7a}$$

$$r_{\varphi\varphi}(z_i,\zeta_k,t) = g_{\varphi}(z_i,\zeta_k)\theta(z_i,\zeta_k,t)\Delta V(z_i)\Delta V(\zeta_k) \tag{7b}$$

$$d_{\varphi\varphi}(z_i,\xi_k,t) = \tilde{g}_{\varphi}(z_i,\xi_k)D^{\alpha}_{0^+}[\theta(z_i,\xi_k,t)]\Delta V(z_i)\Delta V(\xi_k) \tag{7c}$$

where $g_\varphi$ and $\tilde{g}_\varphi$ are the attenuation function of the long range elastic and fractional viscoelastic pure bending interactions, respectively. Typically, these functions are chosen as Gaussian, exponential or power law [12, 16]. The forces mutually exerted by the two volumes $\Delta V(x_i)$ and $\Delta V(\xi_k)$, due to the pure shear defromation $\psi$, are given as:

$$q_y(z_i,\xi_k,t) = r_y(z_i,\xi_k,t) + d_y(z_i,\xi_k,t) \tag{8a}$$

$$r_y(z_i,\xi_k,t) = \frac{1}{|z_i-\xi_k|}g_y(z_i,\xi_k)\psi(z_i,\xi_k,t)\Delta V(z_i)\Delta V(\xi_k) \tag{8b}$$

$$d_y(z_i,\xi_k,t) = \frac{1}{|z_i-\xi_k|}\tilde{g}_y(z_i,\xi_k)D^{\alpha}_{0^+}[\psi(z_i,\xi_k,t)]\Delta V(zx_i)\Delta V(\xi_k) \tag{8c}$$

whereas the moments are

$$q_{\varphi y}(z_i,\xi_k,t) = r_{\varphi y}(z_i,\xi_k,t) + d_{\varphi y}(z_i,\xi_k,t) \tag{9a}$$

$$r_{\varphi y}(z_i,\xi_k,t) = g_y(z_i,\xi_k)\psi(z_i,\xi_k,t)\Delta V(z_i)\Delta V(\xi_k) \tag{9b}$$

$$d_{\varphi y}(z_i,\xi_k,t) = \tilde{g}_y(z_i,\xi_k)D^{\alpha}_{0^+}[\psi(z_i,\xi_k,t)]\Delta V(z_i)\Delta V(\xi_k) \tag{9c}$$

### 2.4 Non-local bar equation of motion

Let us divide the bar in $N$ segments of length $\Delta x$ and consider the bar segment of $\Delta V(x_i) = A\Delta x$ at the location $x = x_i = i\Delta x$, with $i = 0,1,...,N$; the equations of motion of this bar segment are

$$T^{(l)}(z_i+\Delta z) - T^{(l)}(z_i) + R_y(z_i,t) + F_y(z_i,t)\Delta z - \rho(x_i)A\ddot{v}(z_i,t)\Delta z = 0 \tag{10a}$$

$$M^{(l)}(z_i+\Delta z) - M^{(l)}(z_i) + R_\varphi(z_i,t)\Delta z - \rho I_x\ddot{\varphi}(z_i,t)\Delta z = 0 \tag{10b}$$

where $q_y(z_i,t)$ is the external force per unit-length, $m(x) = \rho(x)A$ being $\rho(x)$ the mass per unit volume and $R_y$ and $R_\varphi$ are the resultants of non-local forces and moments on the beam segment at hand. They can be written as

$$R_y(z_i,t) = \sum_{k=0,k\neq i}^{N-1} q_y(z_i,\xi_k,t); \qquad R_\varphi(z_i,t) = \sum_{k=0,k\neq i}^{N-1} q_{\varphi\varphi}(z_i,\xi_k,t) + q_{\varphi y}(z_i,\xi_k,t) \tag{11}$$

By considering Eqs. (11), dividing Eqs. (10) by $\Delta z$ and performing the limit for $\Delta z \to 0$, the continuous counterparts of Eqs. (10) are obtained:

$$\chi GA\left[\frac{\partial^2 u(z,t)}{\partial z^2} + \frac{\partial\varphi(z,t)}{\partial z}\right] + q_y(z,t) + \int_0^L \frac{2}{\xi - z}\left\{g_y(z,\xi)\psi(z,\xi,t) + \right.$$

$$\left. \tilde{g}_y(z,\xi)D^{\alpha}_{0^+}[\psi(z,\xi,t)]\right\}dz = \rho A\ddot{v}(z,t) \tag{12a}$$

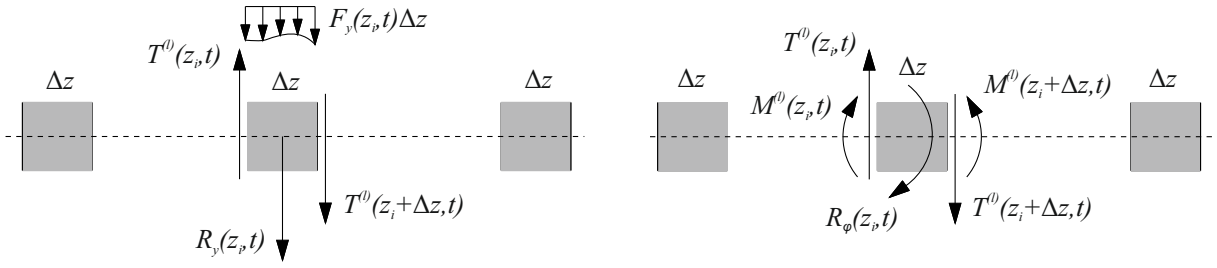


*Figure 3: Translation and rotation equilibrium of a bar segment; positive sign conventions are reported.*

$$EI_x\frac{\partial^2\varphi(z,t)}{\partial z^2}+\chi GA\left[\frac{\partial u(z,t)}{\partial z}+\varphi(z,t)\right]+A^2\int_0^L\left\{g_\varphi(z,\xi)\theta(z,\xi,t)+\tilde{g}_\varphi(z,\xi)D^\alpha_{0^+}\left[\theta(z,\xi,t)\right]\right\}dz+$$

$$A^2\int_0^L\left\{g_y(z,\xi)\psi(z,\xi,t)+\tilde{g}_y(z,\xi)D^\alpha_{0^+}\left[\psi(z,\xi,t)\right]\right\}dz=\rho I_x\ddot{\varphi}(z,t) \quad (12b)$$

Regards the boundary conditions (BCs), it can be easily seen that the BCs of the classical local theory still hold since in the equilibrium equation at the bar ends, the long-range resultants are infinitesimal of higher order with respect to the local resultants [23]. They are not reported here for brevity.

## 2.5 Finite element formulation

The displacement based non-local model of the bar is suitable for implementation in FE method. To this purpose, let us divide the bar in $n$ finite elements of the same length $l$, such that $nl=L$, being $L$ the length of the bar. The points shared by adjacent bar elements are the nodes; the generic $i-th$ element has two nodes located at $z=\hat{z}_i=(i-1)l$ and $z=\hat{z}_{i+1}=il$. The displacement field within the element is approximated by means of standard linear shape functions as follows:

$$u_i(z,t)=\boldsymbol{N}_i(z)\boldsymbol{d}_i(t);\qquad \boldsymbol{d}_i(t)=\left[v_{(i)1}(t)\ \varphi_{(i)1}(t)\ v_{(i)2}(t)\ \varphi_{(i)2}(t)\right] \quad (13)$$

where $i=1,2,...,n,$, $v_{(i)1,2}(t)$ and $\varphi_{(i)1,2}(t)$, are the transverse displacements and rotations of the two nodes of the $i-th$ element and $\boldsymbol{N}_i(x)$ is the shape functions vector of the $i-th$ element, that is

$$\boldsymbol{N}_i(z)=\begin{bmatrix}\frac{(l-y_i)\left(l^2(1+12\Omega)+(l-2y_i)y_i\right)}{l^3(1+12\Omega)} & \frac{6(l-y_i)y_i}{l^3(1+12\Omega)}\\ -\frac{(l-y_i)(l+6l\Omega-y_i)y_i}{l^2(1+12\Omega)} & \frac{(l+12l\Omega-3y_i)(l-y_i)}{l^2(1+12\Omega)}\\ \frac{y_i(12l^2\Omega+3ly_i-2y_i^2)}{l^3(1+12\Omega)} & \frac{6(y_i-l)y_i}{l^3(1+12\Omega)}\\ \frac{(l-y_i)(6l\Omega+y_i)y_i}{l^2(1+12\Omega)} & \frac{(2l(1-6\Omega)+3y_i)y_i}{l^2(1+12\Omega)}\end{bmatrix} \quad (14)$$

where $y_i=z-\hat{z}_i$. Next, being $\boldsymbol{d}^T(t)=\left[u_1(t)\ u_2(t)\dots u_{n+1}(t)\right]^T$ the vector collecting the displacements of all nodes, the nodal displacements of the $i-th$ element are written as $\boldsymbol{d}_i(x)=\boldsymbol{C}_i\boldsymbol{d}(t)$ where $C_i$ is the connectivity matrix of the $i-th$ element. Following a standard Galerkin approach, the dynamic equilibrium equation of the discretized bar is

$$\boldsymbol{M}\ddot{\boldsymbol{d}}(t)+\boldsymbol{C}^{(nl)}\left(D^\alpha\boldsymbol{d}\right)(t)+\boldsymbol{K}\boldsymbol{d}(t)=\boldsymbol{F}(t), \quad (15)$$

being $\boldsymbol{M}$ the consistent mass matrix, $\boldsymbol{C}^{(nl)}$ the matrix of fractional viscoelastic long range interactions, $\boldsymbol{K}$ the stiffness matrix and $\boldsymbol{F}(t)$ the vector of nodal forces. The stiffness matrix is obtained as

$$\boldsymbol{K}=\boldsymbol{K}^{(l)}+\boldsymbol{K}^{(nl)}=\sum_{i=1}^{n}\boldsymbol{K}_i^{(l)}+\sum_{i=1}^{n}\boldsymbol{K}_i^{(nl)}, \quad (16)$$

where $\boldsymbol{K}^{(l)}$ and $\boldsymbol{K}^{(nl)}$ are the local and non-local stiffness contribution to the stiffness, respectively. The local stiffness matrix of the $i-th$ element is

$$\boldsymbol{K}_i^{(l)} = \int_{\hat{z}_i}^{\hat{z}_{i+1}} [\boldsymbol{B}_i(z)\boldsymbol{C}_i]^T \boldsymbol{D}\boldsymbol{B}_i(z)\boldsymbol{C}_i dz, \tag{17}$$

where $\boldsymbol{D} = \mathrm{D}iag\,[EI_x \;\; \chi GA]$ and $\boldsymbol{B}_i(z)$ is the vector collecting the spatial derivative of the shape functions and is not reported here for brevity, while $\boldsymbol{K}_i^{(nl)}$ is evaluated as

$$\boldsymbol{K}_i^{(nl)} = \boldsymbol{K}_i^{(nl,\theta)} + \boldsymbol{K}_i^{(nl,\psi)} = \sum_{j=1}^{n} \boldsymbol{K}_{ij}^{(nl,\theta)} + \sum_{j=1}^{n} \boldsymbol{K}_{ij}^{(nl,\psi)} \tag{18}$$

with

$$\boldsymbol{K}_{ij}^{(nl,\theta)} = \frac{A^2}{2} \int_{\hat{z}_i}^{\hat{z}_{i+1}} \int_{\hat{z}_j}^{\hat{z}_{j+1}} \left[\boldsymbol{N}_j^{(\varphi)}(\zeta)\boldsymbol{C}_j - \boldsymbol{N}_i^{(\varphi)}(z)\boldsymbol{C}_i\right]^T g_\varphi(z,\zeta) \left[\boldsymbol{N}_j^{(\varphi)}(\zeta)\boldsymbol{C}_j - \boldsymbol{N}_i^{(\varphi)}(z)\boldsymbol{C}_i\right] dz d\zeta \tag{19a}$$

$$\boldsymbol{K}_{ij}^{(nl,\psi)} = \frac{A^2}{2} \int_{\hat{z}_i}^{\hat{z}_{i+1}} \int_{\hat{z}_j}^{\hat{z}_{j+1}} \left[2\left(\boldsymbol{N}_j^{(v)}(\zeta)\boldsymbol{C}_j - \boldsymbol{N}_i^{(v)}(z)\boldsymbol{C}_i\right)/(\zeta - z) + \boldsymbol{N}_j^{(\varphi)}(\zeta)\boldsymbol{C}_j + \boldsymbol{N}_i^{(\varphi)}(z)\boldsymbol{C}_i\right]^T$$

$$g_y(z,\zeta) \left[2\left(\boldsymbol{N}_j^{(v)}(\zeta)\boldsymbol{C}_j - \boldsymbol{N}_i^{(v)}(z)\boldsymbol{C}_i\right)/(\zeta - z) + \boldsymbol{N}_j^{(\varphi)}(\xi)\boldsymbol{C}_j + \boldsymbol{N}_i^{(\varphi)}(z)\boldsymbol{C}_i\right] dz d\zeta \tag{19b}$$

It is to emphasized that the matrix $\boldsymbol{C}^{(nl)}$ has the same mathematical form of the non-local stiffness matrix $\boldsymbol{K}^{(nl)}$; the only difference is that in $\boldsymbol{C}^{(nl)}$ $g_i(z,\zeta)$ has been replaced by $\tilde{g}_i(z,\zeta)$. Finally, the vector $\boldsymbol{F}(t)$ is given as:

$$\boldsymbol{F}(t) = \sum_{i=1}^{n} \int_{V_i} [\boldsymbol{N}_i(x)\boldsymbol{C}_i]^T \bar{\boldsymbol{F}}(z,t) dV_i(x) + [\boldsymbol{N}_1(0)\boldsymbol{C}_i]^T \bar{\boldsymbol{F}}_1(t) + [\boldsymbol{N}_{n+1}(L)\boldsymbol{C}_{n+1}]^T \bar{\boldsymbol{F}}_{n+1}(t). \tag{20}$$

where $\bar{\boldsymbol{F}}(z,t) = [F_y(z,t) \;\; 0]$ and $\bar{\boldsymbol{F}}_i(t) = [T_i \;\; M_i]$, $i = 1, n+1$, being $T_i$ and $M_i$ the shear and bending moment reactions.

# 3 Stochastic response of non-local beam

The finite element formulation of fractional viscoelastic non local beam is considered for the case in which the external load vector in Eq. (15) is composed by stochastic actions. An approach to find the analytical solution of the power spectral PSD of the stochastic response of such mechanical system is present below.

## 3.1 Problem formulation in frequency domain

In the stochastic case, the set of coupled differential equations in Eq. (15) is forced by a stochastic input. In particular, consider that each node of the beam is forced by a zero mean Gaussian white noise denoted by $W(t)$, therefore $\bar{\boldsymbol{F}}(t) = \boldsymbol{p}W(t)$, being $\boldsymbol{p}$ an influence vector. In this case the set of inputs are stochastic processes and the response vector is a set of stochastic response processes too $\boldsymbol{d}^T(t) = [V_1(t), \Phi_1(t), \ldots, V_{n+1}(t), \Phi_{n+1}(t)]$. Moreover, since the fractional derivative is a linear operator, and the input processes are Gaussian, than the set of nodal displacements $\boldsymbol{d}(t)$ is composed by Gaussian processes too. Therefore, each response process can be described at steady state by two deterministic function. That is, the PSD, and the CF that are related each other by the Fourier transform.

Without loss of generality, consider the evaluation of the PSD only. Such stationary analysis in frequency domain in terms of PSD determination is particularly useful for the evaluation of the stationary statistics of the response. This aim can be pursued considering the Eq. (15) in frequency domain. In other words, taking into account that the forcing vector contains stochastic processes and performing the Fourier transform, Eq. (15) in frequency domains yields

$$\left[-\omega^2\boldsymbol{M}+(i\omega)^{\alpha}\boldsymbol{C}^{(nl)}+\boldsymbol{K}\right]\boldsymbol{d}_{\mathscr{F}}(\omega,T)=\boldsymbol{p}W_{\mathscr{F}}(\omega,T) \tag{21}$$

where the $i=\sqrt{-1}$ is the imaginary unit, $\boldsymbol{d}_{\mathscr{F}}(\omega,T)$ contains the truncated Fourier transform of the response processes, and $W_F(\omega,T)$ denotes the Fourier transform of the Gaussian white noises truncated at time $T$ in the frequency domain $\omega$. Observe that the power law $(i\omega)^{\alpha}$, related to the fractional order terms, contains an effective stiffness (related to the $\Re[(i\omega)^{\alpha}]$) and an effective damping (proportional to the $\Im[(i\omega)^{\alpha}]$). From Eq. (21) the response in the frequency domain is

$$\boldsymbol{d}_{\mathscr{F}}(\omega,T)=\left[-\omega^2\boldsymbol{M}+(i\omega)^{\alpha}\boldsymbol{C}^{(nl)}+\boldsymbol{K}\right]^{-1}\boldsymbol{p}W_{\mathscr{F}}(\omega,T)=\boldsymbol{H}(\omega)\boldsymbol{p}W_{\mathscr{F}}(\omega,T), \tag{22}$$

where $\boldsymbol{H}(\omega)$ contains the transfer functions.
In order to fully characterize the stationary response in terms of displacements $V_j(t)$ and rotation $\Phi_j(t)$ for $j=1,2,\ldots,n+1$, the evaluation of the PSD and all the cross PSD of each element of the vector $\boldsymbol{d}(t)$ is needed. In this regard, consider the PSD matrix defined as

$$\begin{aligned}\boldsymbol{S}_d(\omega)&=\lim_{T\to\infty}\frac{1}{2\pi T}\mathrm{E}\left[\boldsymbol{H}^*(\omega)\boldsymbol{p}W^*_{\mathscr{F}}(\omega,T)W_{\mathscr{F}}(\omega,T)\boldsymbol{p}^T\boldsymbol{H}^T(\omega)\right]\\&=\boldsymbol{H}^*(\omega)\boldsymbol{p}\lim_{T\to\infty}\frac{1}{2\pi T}\mathrm{E}\left[W^*_{\mathscr{F}}(\omega,T)W_{\mathscr{F}}(\omega,T)\right]\boldsymbol{p}^T\boldsymbol{H}^T(\omega)=\boldsymbol{H}^*(\omega)\boldsymbol{p}S_0\boldsymbol{p}^T\boldsymbol{H}^T(\omega),\end{aligned} \tag{23}$$

where $S_0=S_W(\omega)$ is the constant PSD of the Gaussian white noise, $\mathrm{E}[\cdot]$ is the expectation value, and the apex * denotes the complex conjugate. Consequently, the matrix $\boldsymbol{S}_d(\omega)$ is

$$\boldsymbol{S}_d(\omega)=\begin{bmatrix}S_{V_1}(\omega) & S_{V_1\Phi_1}(\omega) & \ldots & S_{V_1\Phi_{n+1}}\\ S_{\Phi_1V_1}(\omega) & S_{\Phi_1}(\omega) & \ldots & S_{\Phi_1\Phi_{n+1}}\\ \vdots & \vdots & \ddots & \vdots\\ S_{\Phi_{n+1}V_1}(\omega) & S_{\Phi_{n+1}\Phi_1}(\omega) & \ldots & S_{\Phi_{n+1}}\end{bmatrix} \tag{24}$$

and each term represents the PSD function of the output processes and their cross counterparts. In particular, the diagonal terms are the PSDs, whereas the other terms are the cross PSDs. Unfortunately, the PSD matrix cannot be obtained in analytical form because the matrix $\boldsymbol{H}(\omega)$ cannot be obtained by means of the matrix inversion in Eq. (22). In fact, just a numerical evaluation of each terms of $\boldsymbol{S}_d(\omega)$ can be pursued by the discretization of the variable $\omega$. For this reason in the next subsection the problem is solved with the introduction of a proper state variable expansion and a complex modal transformation in order to find the exact solution of each term in the PSD matrix. However, the numerical solution obtained with the aid of of Eq. (22) is used as a benchmark for the results obtained by the method in the next subsection.

### 3.2 State variable expansion and complex modal exapnsion

The matrix inversion problem in the previous subsection in some cases can be overcame with the aid of a classical modal transformation and diagonalizing all the involved matrices in Eq. (21). Unfortunately, for the case at hand the three involved matrices can be diagonalized and other

mathematical tools are needed. In this regards, consider the case in which the fractional order $\alpha$ is rational, under this assumptions it is possible to represent the generic fractional order as irreducible fractions of two integer values $\alpha = a/b$, where $a, b \in \mathbb{N}$. Thus, the system in Eq. (21) can be rewritten as the following sequential linear algebraic equations:

$$\left[\sum_{j=1}^{2b} \boldsymbol{C}_j (i\omega)^{j/b} + \boldsymbol{K}\right] \boldsymbol{d}_{\mathscr{F}}(\omega, T) = \boldsymbol{v} W_{\mathscr{F}}(\omega, T), \tag{25}$$

where the involved matrices in the summation are $\boldsymbol{C}_a = \boldsymbol{C}^{(nl)}$, $\boldsymbol{C}_{2b} = \boldsymbol{M}$ and $\boldsymbol{C}_j = \boldsymbol{0}$, $\forall j : j \in (1, a]\, and\, [a, 2b-1)$. Introducing the vector of state variables in the frequency domain

$$\boldsymbol{z}^{\mathrm{T}}_{\mathscr{F}}(\omega, T) = \left[\boldsymbol{d}^{\mathrm{T}}_{\mathscr{F}}(\omega, T),\ (i\omega)^{1/b} \boldsymbol{d}^{\mathrm{T}}_{\mathscr{F}}(\omega, T),\ \ldots\ (i\omega)^{(2b-1)/b} \boldsymbol{d}^{\mathrm{T}}_{\mathscr{F}}(\omega, T)\right], \tag{26}$$

and appending to Eq. (25) the $2b-1$ identities

$$\sum_{j=1}^{2b-k} \boldsymbol{C}_{j+k} (i\omega)^{1/b} (i\omega)^{(j-1)/b} \boldsymbol{d}^{\mathrm{T}}_{\mathscr{F}}(\omega, T) = \sum_{j=1}^{2b-k} \boldsymbol{C}_{j+k} (i\omega)^{j/b} \boldsymbol{d}^{\mathrm{T}}_{\mathscr{F}}(\omega, T), \quad k = 1, 2, \ldots, 2b-1, \tag{27}$$

then a set of $(n+1) \times 2b$ coupled algebraic equations is readily cast in the form

$$\left(\boldsymbol{A} \sqrt[b]{i\omega} + \boldsymbol{B}\right) \boldsymbol{z}_{\mathscr{F}}(\omega, T) = \boldsymbol{g}_{\mathscr{F}}(\omega, T), \tag{28}$$

where $\boldsymbol{g}_{\mathscr{F}}(\omega, T) = W_{\mathscr{F}}(\omega, T) \left[\boldsymbol{v}^T\ \boldsymbol{0}\ \ldots\ \boldsymbol{0}\right]$, the involved matrices are symmetric and defined as

$$\boldsymbol{A} = \begin{bmatrix} \boldsymbol{C}_1 & \boldsymbol{C}_2 & \ldots & \boldsymbol{C}_{2b-1} & \boldsymbol{C}_{2b} \\ \boldsymbol{C}_2 & \boldsymbol{C}_3 & \ldots & \boldsymbol{C}_{2b} & \boldsymbol{0} \\ \vdots & \vdots & \ddots & \vdots & \vdots \\ \boldsymbol{C}_{2b-1} & \boldsymbol{C}_{2b} & \ldots & \boldsymbol{0} & \boldsymbol{0} \\ \boldsymbol{C}_{2b} & \boldsymbol{0} & \ldots & \boldsymbol{0} & \boldsymbol{0} \end{bmatrix} \quad \boldsymbol{B} = \begin{bmatrix} \boldsymbol{K} & \boldsymbol{0} & \ldots & \boldsymbol{0} & \boldsymbol{0} \\ \boldsymbol{0} & -\boldsymbol{C}_2 & \ldots & -\boldsymbol{C}_{2b-1} & -\boldsymbol{C}_{2b} \\ \vdots & \vdots & \ddots & \vdots & \vdots \\ \boldsymbol{0} & -\boldsymbol{C}_{2b-1} & \ldots & \boldsymbol{0} & \boldsymbol{0} \\ \boldsymbol{0} & -\boldsymbol{C}_{2b} & \ldots & \boldsymbol{0} & \boldsymbol{0} \end{bmatrix}. \tag{29}$$

Now, it is possible to diagonalize the involved matrix by placing the complex modal transformation $\boldsymbol{y}_{\mathscr{F}}(\omega, T) = \boldsymbol{\Psi} \boldsymbol{z}_{\mathscr{F}}(\omega, T)$. That is,

$$\begin{gathered} \boldsymbol{\Psi}^{\mathrm{T}} \left(\boldsymbol{A} \sqrt[b]{i\omega} + \boldsymbol{B}\right) \boldsymbol{\Psi}\, \boldsymbol{y}_{\mathscr{F}}(\omega, T) = \boldsymbol{\Psi}^{\mathrm{T}} \boldsymbol{g}_{\mathscr{F}}(\omega, T) \\ \left(\boldsymbol{U}_{\mathbf{d}} \sqrt[b]{i\omega} + \boldsymbol{V}_{\mathbf{d}}\right) \boldsymbol{y}_{\mathscr{F}}(\omega, T) = \boldsymbol{\mu}_{\mathscr{F}}(\omega, T), \end{gathered} \tag{30}$$

where $\boldsymbol{\Psi}$ contains the eigenvectors of the matrix $\boldsymbol{D} = \boldsymbol{A}^{-1}\boldsymbol{B}$, the matrices $\boldsymbol{U}_{\mathbf{d}} = \boldsymbol{\Psi}^{\mathrm{T}} \boldsymbol{A} \boldsymbol{\Psi}$ and $\boldsymbol{V}_{\mathbf{d}} = \boldsymbol{\Psi}^{\mathrm{T}} \boldsymbol{B} \boldsymbol{\Psi}$ are diagonal (the subscript $\mathbf{d}$ stands for diagonal). Now, from Eq. (30) the response in the complex modal space is

$$\boldsymbol{y}_{\mathscr{F}}(\omega, T) = \left(\boldsymbol{U}_{\mathbf{d}} \sqrt[b]{i\omega} + \boldsymbol{V}_{\mathbf{d}}\right)^{-1} \boldsymbol{\mu}_{\mathscr{F}}(\omega, T) = \boldsymbol{H}_{\mathbf{d}}(\omega) \boldsymbol{\mu}_{\mathscr{F}}(\omega, T), \tag{31}$$

since the matrix $\boldsymbol{H}_{\mathbf{d}}(\omega) = (\boldsymbol{U}_{\mathbf{d}} \sqrt[b]{i\omega} + \boldsymbol{V}_{\mathbf{d}})^{-1}$ can be evaluated in closed form each term of the vector $\boldsymbol{\mu}_{\mathscr{F}}(\omega, T)$ can be readily obtained and then the exact PSD matrix in the state variable

domain can be derived. In particular,

$$\begin{aligned}\boldsymbol{S}_{\boldsymbol{z}}(\omega) &= \boldsymbol{\Psi} \lim_{T\to\infty} \frac{1}{2\pi T} \mathrm{E}\left[\boldsymbol{z}^*_{\mathscr{F}}(\omega,T)\boldsymbol{z}^{\mathrm{T}}_{\mathscr{F}}(\omega,T)\right] \\ &= \boldsymbol{\Psi} \lim_{T\to\infty} \frac{1}{2\pi T} \mathrm{E}\left[\boldsymbol{H}^*(\omega)\boldsymbol{p} W^*_{\mathscr{F}}(\omega,T) W_{\mathscr{F}}(\omega,T)\boldsymbol{p}^T\boldsymbol{H}^T(\omega)\right] \\ &= \boldsymbol{H}^*(\omega)\boldsymbol{p} \lim_{T\to\infty} \frac{1}{2\pi T} \mathrm{E}\left[W^*_{\mathscr{F}}(\omega,T) W_{\mathscr{F}}(\omega,T)\right] \boldsymbol{p}^T\boldsymbol{H}^T(\omega) = \boldsymbol{H}^*(\omega)\boldsymbol{p}S_0\boldsymbol{p}^T\boldsymbol{H}^T(\omega),\end{aligned} \tag{32}$$

The described state variable analysis and the complex modal transformation are used in the next section to investigate the influence of the fractional order on the statistics of stationary and non-stationary response.

# 4 Numerical applications

The state variable expansion described in the previous section is used now to evaluate the statistics of the stochastic response of the non-local bar forced by Gaussian white noise. In particular, the cantilever rod is forced by Gaussian white noise acceleration impressed at the fixed end in axial direction. Such white noise is characterized by unitary PSD, $S_0 = 1$. The mechanical element is an epoxy micro beam with longitudinal length $L = 300\,\mu m$. The bar has a constant cross section with dimensions $b = 30\,\mu m$ and $h = 15\,\mu m$. Considering that the material is an epoxy resin the elastic modulus is $E = 1.4\,GPa$, whereas the density is $\rho = 1000\,Kg/m^3$. As for the attenuation functions, typical exponential functions have been selected [16, 20]. That is,

$$g(x,\xi) = \frac{C}{h^2}\exp\left(\frac{|x-\xi|}{\lambda}\right), \tag{33a}$$

$$\tilde{g}(x,\xi) = \frac{\tilde{C}}{h^2}\exp\left(\frac{|x-\xi|}{\tilde{\lambda}}\right), \tag{33b}$$

where $\lambda = \tilde{\lambda} = 30\ \mu m$, $C = 10^{22}\ Nm^{-6}$ and $\tilde{C} = 10^{21}\ Nm^{-6}$. For the finite element formulation the bar is divided in forty parts and then $n = 40$ nodes are considered. In order to show the effect of the fractional order in the stochastic response of the bar, two different cases are considered. In the first case the chosen fractional order is $\alpha = 1/4$, whereas in the second case the fractional order is $\alpha = 3/4$. Such choice aims to show the differences between the response in the case in which the elastic phase is predominant (elasto-viscous (EV) case $\alpha = 1/4$) and the response when the damping effect prevails (visco-elastic (VE) case $\alpha = 3/4$). In both cases the matrices of the coefficients $\boldsymbol{C}_{nl}$ are the same. In this manner only the influence of the fractional order is considered.

For both cases the value $b$ in Eq. (25) that allows to rewrite the equation of motion in the state variables domain is $b = 4$ and the number of state variables is $2b = 8$.

By performing the state variable expansion and the complex modal transformation, the Eq. (**??**) gives each nodal displacements $U_j(t)$ for any generic sample of the Gaussian white noise $W(t)$. Such samples have been simulated by the harmonic superposition method by Shinozuka and Deodatis [24]. The number of generated sample for the Monte Carlo simulation is $N = 2000$. The time step chosen to generate the samples of $W(t)$ and for the numerical integration of Eq. (**??**) and the total duration of the simulation $t_f$ have been calibrated in such a way that the stationary condition are reached. For this reason in the case $\alpha = 1/4$ the time step is $\Delta t = 10^{-8}\,s$ and $t_f = 10^{-5}\,s$, while in the case $\alpha = 3/4$ $\Delta t = 10^{-6}\,s$ and $t_f = 5\times 10^{-4}\,s$. After the generation of the input and the numerical integration of the Eq. (**??**) the statistics can be evaluated at the

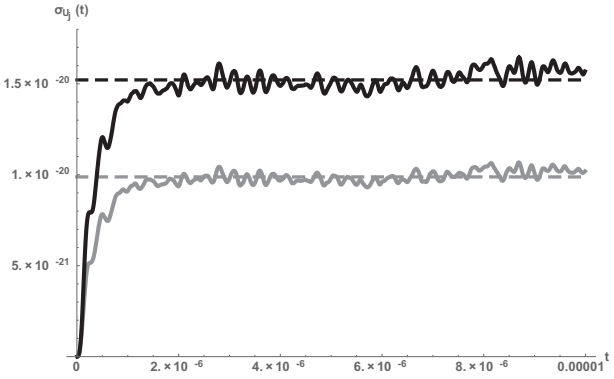


*Figure 4: Displacement variance at $x = L$ (black) and $x = L/2$ (gray) for EV case $\alpha = 1/4$.*

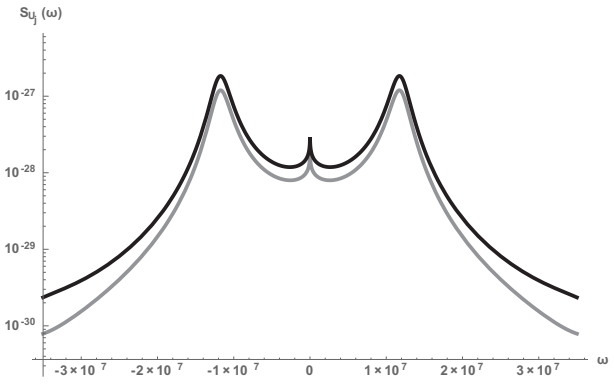


*Figure 5: PSD of axial displacement at $x = L$ (black) and $x = L/2$ (gray) for EV case $\alpha = 1/4$.*

different nodes. In particular, the considered nodes are the middle-bar node and the free end one.

The stationary and non-stationary variance of the two considered displacements for $\alpha = 1/4$ are reported in Figure 4, while the results for $\alpha = 3/4$ are reported in Figure 6. These results are compared with the stationary variances obtained by numerical integration of the PSD functions of the Eq. (23) and depicted in dotted line in Figure 4 for the EV case and in Figure 6 for the VE case.

The PSD of the two considered displacements are reported in Figure 5 for the EV case and in Figure 7 for the VE case.

Comparing the stationary variances and the PSD functions of both EV and VE case some useful consequences can be drawn. In particular, the increasing of the fractional order leads to a

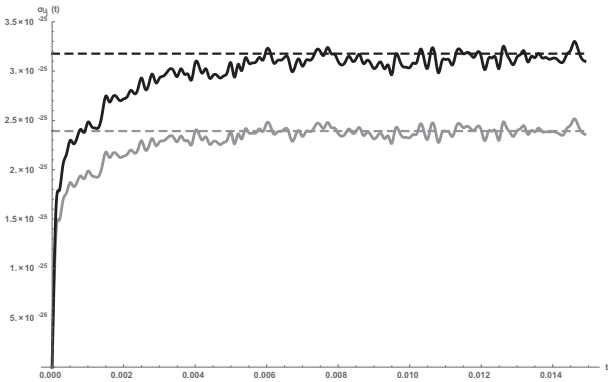


*Figure 6: Displacement variance at $x = L$ (black) and $x = L/2$ (gray) for VE case $\alpha = 3/4$.*

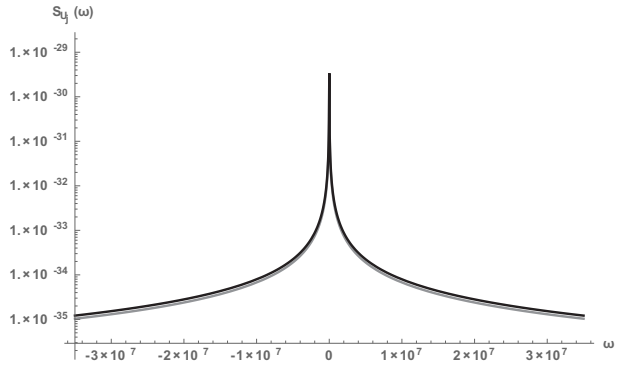


*Figure 7: PSD of axial displacement at $x = L$ (black) and $x = L/2$ (gray) for VE case $\alpha = 3/4$.*

reduction of the PSD amplitude. This is related to the increment of damping effect in the frequency domain, in fact when $\alpha$ grows, then the imaginary part of the power law term $(i\omega)^\alpha$ in Eq. (22) increases. Such reduction can be observed comparing the PSDs in Figure 5 and 7 and considering the peaks for $\alpha = 1/4$ in Fig. 5 that do not exist in the other case depicted in Fig. 7. Obviously, it implies that when the fractional order increases the stationary variance decreases.

# 5 Concluding remarks

The noisy non-local bar with fractional order term is a practical example of real mechanical problem in which the classical modal transformation fails to decouple the system of fractional differential equations that rules the motion. For this reason in this paper a method to decouple the equations of motion when fractional order terms appear has been introduced.
The bar has been discretized with the FE formulation of the nonlocal beams provided by the authors in previous papers which closed form matrices are available. Once the FE model of the bar has been constructed it can be treated as a generic fractional multi-degree of freedom system. The described state variable expansion and the complex modal transformation have allowed to integrate the solution in the time domain and also to perform Monte Carlo simulation very efficiently.
The study has been focused to the evaluation of the effect of the fractional order on the statistics of the response. In particular, the influence of the fractional order on the PSD response has been investigated. The numerical results, corroborated by the Monte Carlo simulation, have been shown that the increasing of the fractional order leads to a reduction of the amplitude of the PSD function.

# References

[1] Lakes, R.S., 1991. Experimental micro mechanics methods for conventional and negative Poissons ratio cellular solids as Cosserat continua. *Journal of Engineering Materials and Technology*, **113**(1), pp. 148155.

[2] Arash, B., and Wang, Q. 2012. A review on the application of nonlocal elastic models in modeling of carbon nanotubes and graphenes. *Computational Materials Science*, **51**(1), pp. 303313.

[3] Wang, L. F., and Hu, H. Y., (2005). Flexural wave propagation in single-walled carbon nanotube. *Physical Review B*, **71**(19), pp. 195412195418.

[4] Lam, D.C.C., Yang, F., Chong, A.C.M., Wang, J., and Tong, P., 2003. Experiments and

theory in strain gradient elasticity. *Journal of Mechanics and Physics of Solids*, **51**(8), pp. 14771508.

[5] Eringen, A.C., 1972. Linear theory of non-local elasticity and dispersion of plane waves. *International Journal Engineering Science*, **10**(5), pp. 425435.

[6] Lu, P., Lee, H.P., Lu, C., and Zhang, P.Q., 2007. Application of nonlocal beam models for carbon nanotubes. *International Journal of Solids and Structures*, **44**(16), pp. 52895300.

[7] Payton, D., Picco, L., Miles, M.J., Homer, M.E., and Champneys, A.R., 2012. Modelling oscillatory flexure modes of an atomic force microscope cantilever in contact mode whilst imaging at high speed. *Nanotechnology*, **23**(26), pp. 265702.

[8] Murmu, T., and Adhikari, S., 2012. Nonlocal frequency analysis of nanoscale biosensors. *Sensor and Actuators A-Physical*, **173**(1), pp. 4148.

[9] Chen, C., Ma, M., Liu, J., Zheng, Q., and Xu, Z., 2011. Viscous damping of nanobeam resonators: Humidity, thermal noise, and a paddling effect. *Journal of Applied Physics*, **110**(3), pp. 034320.

[10] Lee, J., and Lin, C., 2010. The magnetic viscous damping effect on the natural frequency of a beam plate subject to an in-plane magnetic field. *Journal of Applied Mechanics*, **77**(1), pp. 011014.

[11] Lei, Y., Friswell, M.I., and Adhikari, S., 2006. A Galerkin method for distributed systems with non-local damping. *International Journal of Solids and Structures*, **43**(1112), pp. 33813400.

[12] Friswell, M.I., Adhikari, S., and Lei, Y., 2007. Non-local finite element analysis of damped beams. *International Journal of Solids and Structures*, **44**(2223), pp. 75647576.

[13] Di Paola, M., Failla, G., and Zingales, M., 2013. Non-local stiffness and damping models for shear-deformable beams. *European Journal of Mechanics A/Solids*, **40**, pp. 6983.

[14] Di Paola, M., Failla, G., and Zingales, M., 2014. Mechanically based nonlocal Euler-Bernoulli beam model. *Journal of Micromechanics and Microengineering*, 10.1061/(ASCE)NM.2153-5477.0000077, A4013002.

[15] Failla, G., Sofi, A., and Zingales, M., 2015. A new displacement-based framework for non-local Timoshenko beams. *Meccanica*, **50**(8), pp. 21032122.

[16] Alotta, G., Failla, G., and Zingales, M., 2014. Finite element method for a nonlocal Timoshenko beam model. *Finite Element in Analysis and Design*, **89**, pp. 77-92.

[17] Alotta, G., Di Paola, M., Pirrotta, A., 2014. Fractional TajimiKanai model for simulating earthquake ground motion. *Bulletin of Earthquake Engineering*, **12**, pp. 2495–2506.

[18] Di Paola, M., Fiore, V., Pinnola, F.P., and Valenza, A., 2014. On the influence of the initial ramp for a correct definition of the parameters of fractional viscoelastic materials. *Mechanics of Materials*, **69**(1), pp. 6370.

[19] Podlubny, I., 1999. *Fractional differential equations: An introduction to fractional derivatives, fractional differential equations, some methods of their solution and some of their applications*. Academic Press, New York.

[20] Alotta, G., Failla, G., and Zingales, M., 2015. Finite-Element Formulation of a Nonlocal Hereditary Fractional-Order Timoshenko Beam. *Journal of Engineering Mechaincs (ASCE)*, 10.1061/(ASCE)EM.1943-7889.0001035.

[21] Pinnola, F.P., 2016. Statistical correlation of fractional oscillator response by complex spectral moments and state variable expansion. *Communications in Nonlinear Science and Numerical Simulation*, **39**, pp. 343–359.

[22] Fuchs, M.B., 1997. Unimodal formulation of the analysis and design problems for framed structures. *Computers and Structures*, **63**(4), pp. 739747.

[23] Di Paola, M., Failla, G., and Zingales, M., 2009. Physically-based approach to the mechanics of strong non-local linear elasticity theory. *Journal of Elasticity*, **97**(2), pp. 103130.

[24] Shinozuka, M., Deodatis, G. 1988. Stochastic process models for earthquake ground motion. *Probabilistic Engineering Mechanics*, **3**, pp. 114–123.